Stationary Vortex Loops Induced by Filament Interaction and Local Pinning in a Chemical Reaction-Diffusion System

Zulma A. Jiménez and Oliver Steinbock

Phys. Rev. Lett. **109**, 098301 — Published 27 August 2012

DOI: 10.1103/PhysRevLett.109.098301

Stationary Vortex Loops Induced by Filament Interaction and Local Pinning in a Chemical Reaction-Diffusion System

Zulma A. Jiménez and Oliver Steinbock

Florida State University, Department of Chemistry and Biochemistry, Tallahassee, Florida 32306-4390

(Dated: July 6, 2012)

Abstract

Scroll rings are three-dimensional excitation waves rotating around one-dimensional filament loops. In experiments with the Belousov-Zhabotinsky reaction we show that the collapse of these loops can be stopped by local pinning to only two unexcitable heterogeneities. The resulting vortices rotate around stationary but curved filaments. The absence of filament motion can be explained by repulsive interaction that counteracts the expected curvature-induced motion. The shape and key dependencies of the stationary filaments are well described by a curvature-flow model with additive interaction velocities that rapidly decrease with filament distance.

PACS numbers: 05.45.-a, 82.40.Ck, 82.40.Qt

Many nonequilibrium systems self-organize macroscopic structures from interactions at the atomic or molecular level. The emergence of this dynamic order often reveals fundamental universalities that span through physics, chemistry, and biology. A prominent example are rotating vortex structures. They occur in systems such as type II superconductors [1], superfluids like ^{4}He [2], Bose-Einstein condensates [3], and chemical as well as biological reaction-diffusion (RD) media.

Spiral waves in two-dimensional RD systems have been observed in system as diverse as catalytic surface reactions [4] and colonies of giant honey bees [5]. They have particle-like features and carry a topological charge that controls short-range interaction, annihilation as well as the formation of intricate bound states [6–8]. Scroll waves are the three-dimensional analogs of spiral waves [9]. By comparison, scroll waves are clearly understudied and numerous fundamental questions concerning their dynamics remain unanswered. In addition, they exist in important systems such as the model organism *Dictyostelium* [10], possibly the cerebral cortex [11], and the human heart [12] where they induce tachycardia and sudden cardiac death [13, 14].

Scroll waves rotate around one-dimensional phase singularities called filaments. The velocities of these curves are well described by the product of their local curvature and a system-specific constant called filament tension α [15]. Accordingly, circular filament loops collapse in finite times ($\alpha > 0$). Furthermore, their motion can be influenced by variations in rotation phase (twist) and by external perturbations such as stationary temperature gradients and electric fields [16, 17]. Of great fundamental interest is the interaction of filaments, which should be dynamical richer than the interaction of point-like spiral cores. To date, however, only a few computational studies have addressed this phenomenon. For instance, Bray and Wikswo showed that mirror-image-like pairs of scroll rings attract or repel each other with distance-dependent velocities that are well described by the difference of two Yukawa potentials [18]. Furthermore, Gabbay *et al.* showed that, in the complex Ginzburg-Landau equation, local attraction between scroll waves can induce filament reconnections [19]. Interaction should also be relevant to turbulence arising from negative filament tension [20] and could explain intermittently forming triple filament strands [21].

In this Letter, we report the first experimental evidence for filament interaction in an excitable reaction-diffusion system. Our results reveal the formation of vortex structures in which neighboring filament branches are stationary despite strong curvature. The experi-

mental preparation of these states relies on recent advances that allow the pinning of scroll waves to inert and impermeable heterogeneities [22–24]. A comparison with curvature-flow simulations yields quantitative information on the distance-dependence of filament interaction.

Our experiments employ the autocatalytic Belousov-Zhabotinsky (BZ) reaction [9] which is a frequently studied model for spiral and scroll waves in excitable RD systems. The reaction system consists of a bottom gel layer and a top liquid layer (each 4 mm thick). The initial concentrations in the two layers are essentially identical: $[H_2SO_4]$= 0.16 mol/L, $[NaBrO_3]$ = 0.04 mol/L, [malonic acid] = 0.04 mol/L, and $[Fe(phen)_3SO_4]$ = 0.5 mmol/L. At the given gel composition (0.8% w/v agar), also all diffusion coefficients are expected to be homogeneous. The filament tension in this system is $\alpha = 1.4 \times 10^{-5}$ cm^2/s and does not depend on the layer height h for $h = 4$ mm and above. During the gelation process, we embed two spherical glass beads halfway into the gel. After completion of gelation, we add the liquid layer and, using the tip of a silver wire, initiate a chemical wave at the midpoint between the beads. Then the solution is agitated which creates a homogeneous, excitable upper layer but does not affect the expansion of a half-spherical wave in the gel. Once the wave reaches the beads, we stop the mechanical agitation and all fluid flow ceases. Subsequently, the rim of the half-spherical wave curls up into the top layer and nucleates a scroll ring pinned to the glass beads [23]. We monitor the experimental system with a CCD camera (equipped with a dichroic blue filter) mounted over the BZ system. Wave patterns can be observed for more than six hours. Image contrast results from the absorption of light by the chemically reduced catalyst. All experiments are carried out at 21.5°C.

Figure 1 shows a representative example of a scroll ring stabilized by pinning to two spherical heterogeneities. Bright and dark areas correspond to dynamically excited and excitable regions, respectively. The largest portion of the wave field propagates in an outward direction; however, within the central region, the waves move inwards and collide in (b) along the horizontal line that connects the two beads. The beads can be discerned as two bright disks while the smaller, dark spots are gas bubbles formed by the reaction product CO_2. For the given system, a free scroll ring of this initial radius ($R_0 = 0.39$ cm) collapses and self-annihilates within $R_0^2/(2\alpha) = 91$ min. The images in (a) and (b), however, show the vortex structure 2 min and 200 min after initiation. This stabilization occurs only above a critical distance of $\Delta_{crit} = 6$ mm between the pinning bead centers. In addition, we found

that the bead radius has to exceed a critical value of $R_{crit} \approx 0.5$ mm to pin the filament. Additional experiments reveal that the latter value is similar to the characteristic core radius (0.4-0.5 mm) of unpinned, two-dimensional spiral waves in this BZ system.

Figure 1(c) shows the reconstructed filament (open small circles) for the vortex in (b). The two large circles indicate the pinning spheres. The stationary filament is clearly deformed from its initial circular shape and well approximated by the arc-shaped lines which are the result of model calculations (see later sections). The structure in Figs. 1(b) and (c) results from a continuous relaxation process which is illustrated by the time-space plot in Fig. 1(d). The latter figure consists of a stack of consecutive image profiles that we obtained along the bright (yellow) line in Fig. 1(a). Time evolves in downward direction. The two intersections of the filament with the line appear in (d) as Λ-shaped kinks which correspond to points of abrupt change in wave direction.

From these data one can readily obtain the position and time-dependent filament distance $d(x,t)$. Notice that the x-axis connects the pinning sites and $x = 0$ denotes their midpoint (see Fig. 1(c)). Figure 2 shows three representative examples of the maximal filament distance $d(0,t)$. The examples differ in the distance Δ between the pinning beads and also in the initial value d_0. For a perfectly circular, initial filament $\Delta = d_0$. The experimental data are well described by compressed exponentials of the form

$$d(0,t) = d_{ss} + (d_0 - d_{ss})\ e^{-(t/\tau)^{\beta}}, \tag{1}$$

where d_{ss}, τ, and β denote the maximal filament distance in the stationary state, a characteristic relaxation time, and the compression exponent, respectively. Notice that this result differs profoundly from the dynamics of unpinned, circular filaments which are known to obey $d(t) = \sqrt{d_0^2 - 8\alpha t}$ [16, 25]. Analyses of numerous data sets yielded an average β value of about 1.4 and relaxation times τ in the range of 30 min to 140 min. The stationary filament distance d_{ss}, however, depends strongly on the bead distance Δ and the bead radius R. Figure 3 shows that d_{ss} increases with increasing values of Δ but decreases with increasing bead radii. These results also show that the eccentricity of the stationary, lens-shaped filament is largest for large beads but only mildly affected by the bead distance.

Another experimental observable is the angle ϕ between the two filament branches close to the bead surface. Notice that filaments are expected to terminate at no-flux boundaries in normal direction. Very strong repulsion could drive the filaments to antipodal points

($\phi = 180°$) while weaker repulsion would yield smaller ϕ values. Figure 4(a) shows the steady-state values of ϕ as a function of Δ for a constant bead radius of $R = 1.0$ mm. We find that ϕ_{ss} increases with increasing anchor distances and then saturates at an angle of about 140° for distances above 10 mm. The data in Fig. 4(b) show that ϕ_{ss} decreases with increasing anchor radii. The meaning of the continuous lines and the inset in Figs. 3,4 will be explained in the following.

The existence of a stationary filament state suggests a mechanism that counteracts the curvature-induced motion of the filament. In other words, every point along the filament must experience an additional velocity contribution that fully balances the velocity of the free curvature flow. We propose that this velocity is generated by the wave-mediated interaction between the two filament arches. We further assume that this interaction velocity V_i is a function of the position-dependent filament distance $d(x,t)$. To study whether this mechanism could explain the observed stationary solutions and specifically their dependencies on key experimental parameters, we modify the classical description of free filament motion $\mathrm{d}\mathbf{s}/\mathrm{d}t = (\alpha\hat{\mathbf{N}} + \beta\hat{\mathbf{B}})\kappa$, where $\mathbf{s}$, t, κ, $\hat{\mathbf{N}}$, and $\hat{\mathbf{B}}$ denote the filament's position vectors, time, local curvature, unit normal vector, and unit binormal vector, respectively. This kinematic model has been shown to be in excellent agreement with experimental data [16, 25] and can be derived from reaction-diffusion equations in the limit of small curvature and twist [15, 26]. In addition, we reported earlier that for the given BZ medium motion in binormal direction is negligible ($\beta \approx 0$) [23]. Because the initial filament in our experiments is planar and there is no evidence for pinning-induced deformations out of the initial filament plane, we limit our model to a two-dimensional description. For the specific model equation we choose one of the simplest possibilities

$$\frac{\mathrm{d}\mathbf{s}}{\mathrm{d}t} = (\alpha\kappa - V_i)\hat{\mathbf{N}}. \tag{2}$$

Notice that the latter equation ignores potentially relevant factors such as the relative rotation phase of the filament branches, the angle between their tangential vectors, as well as the position and shape of the collision surface between their wave fields. We also limit our discussion to filament pairs of opposite, rotational orientation which corresponds to the situation in our experiments.

Based on the known behavior of two-dimensional vortices in excitable media, one can expect that the interaction velocity $V_i(d)$ decays rapidly with increasing distances between

the filament branches and should become irrelevant at distances above 1.5-2 vortex wavelengths. One can further speculate that V_i changes sign at a much shorter distance because the stationary states in Fig. 1 are caused by repulsive interaction while at very short distances filaments can mutually annihilate and possibly reconnect. In the following, we consider three simple functions: Coulomb-like behavior $V_{i,H} = \delta_H/d$, exponential decay $V_{i,E} = v_E \exp(-k_E d)$, and the difference between two independent Yukawa potentials $V_{i,Y} = \delta_{Y_1} \exp(-k_{Y_1} d)/d - \delta_{Y_2} \exp(-k_{Y_2} d)/d$. All δ's and k's as well as v_E will be treated as fitting parameters. Only $V_{i,Y}$ can change sign. Notice that $V_{i,Y}$ was originally suggested by Bray and Wikswo for the description of interacting scroll ring pairs in an Oregonator model of the BZ reaction [18].

We numerically integrate Eq. (2) for all points along the filament using forward Euler integration and employ half circles of diameter Δ as initial conditions for $\mathbf{s}$. After each iteration, the curve is reparameterized to maintain a constant arclength-resolution of 25 μm. The integration time step is 25 ms. The boundary conditions enforce that the filaments terminate in normal direction to the edge of the pinning, circular anchors. Fitting of our experimental data to these functions yields best agreement for $\delta_H = 1.24 \times 10^{-5}$ cm^2/s, $v_E = 1.08 \times 10^{-4}$ cm/s, $\delta_{Y_1} = 1.468 \times 10^{-4}$ cm^2/s, $\delta_{Y_2} = 1.474 \times 10^{-4}$ cm^2/s, $k_E = 2.6$ cm^{-1}, $k_{Y_1} = 2.271$ cm^{-1}, and $k_{Y_2} = 3.025$ cm^{-1}. Our fitting parameters for the Yukawa functions are of the same order of magnitude as those reported in Ref. [18]; for instance, our $\delta_{Y1,2}$ are only 1.5 to 2.5 times larger than their values. Notice that the BZ concentrations considered in this earlier, computational work differ from the ones studied here.

All smooth curves in Figs. 1(c), 3, 4 are computational results obtained for the latter parameter values. Depending on the choice of the interaction function, these curves are plotted as thick solid ($V_{i,H}$), dashed ($V_{i,E}$), or thin solid lines ($V_{i,Y}$). Overall we find very good agreement between our experimental and computational data. The lack of marked dependencies on the choice of the interaction function is closely related to the small range of d values accessed in our experiments. The inset of Fig. 3(a) shows the three interaction functions for the fitted parameters emphasizing the need for further data at smaller distances. At such distances, however, we do not observe stationary filaments and the vortex structures annihilate. This result is indicative of non-repulsive–and possibly attractive–interaction between the filament arches and hence consistent with our overall description.

Our findings show that the simple model in Eq. (2) is capable of accounting for the shape

and dependencies of the experimentally observed stationary filaments. However, additional experiments and simulations are needed to explore the limits of a description of filament interaction in terms of filament distances alone. Such limitations are likely to exist because the interaction is fully controlled by concentration patterns which are not uniquely defined by the filaments. Moreover, our results raise new questions regarding the fundamental nature of scroll wave pinning. For instance, one can question the validity of our description of the filament loop as two separate filament branches. Such an approach seems appropriate for heterogeneities larger than the characteristic vortex wavelength because such heterogeneities should terminate the phase singularity in the same way as an external boundary [27]. Smaller heterogeneities, like the ones studied here, however, could truly pin the filament without surface-bound termination. Accordingly the scroll's rotation backbone would continue through the anchor and resist local curvature at the pinning site. This stiffness could be an alternative explanation of or contributing factor to the dependencies of ϕ_{ss} in Fig. 4.

This material is based upon work supported by the National Science Foundation under Grant No. 0910657. We thank Sumana Dutta and Laszlo Roszol for discussions.

[1] G. Blatter, M. V. Feigel'man, V. B. Geshkenbein, and A. I. Larkin, Rev. Mod. Phys. **66**, 1125 (1994).

[2] M. Tsubota and S. Maekawa, Phys. Rev. B **47**, 12040 (1993).

[3] M. R. Matthews, B. P. Anderson, P. C. Haljan, D. S. Hall, C. E. Wieman, and E. A. Cornell, Phys. Rev. Lett. **83**, 2498 (1999).

[4] G. Ertl, Angew. Chem. Int. Ed **47**, 3524 (2008).

[5] G. Kastberger, E. Schmelzer, and I. Kranner, PLoS ONE **3**, e3141 (2008).

[6] E. A. Ermakova, A. M. Pertsov, and E. E. Shnol, Physica D **40**, 185 (1989).

[7] O. Steinbock, J. Schütze, and S. C. Müller, , Phys. Rev. Lett. **68**, 248 (1992).

[8] I. Schebesch and H. Engel, Phys. Rev. E**60**, 6429 (1999).

[9] A. T. Winfree, Science **181**, 937 (1973).

[10] O. Steinbock, F. Siegert, S. C. Müller, and C. J. Weijer, Proc. Natl. Acad. Sci. USA **90**, 7332 (1993).

[11] X. Huang, W. Troy, Q. Yang, H. Ma, C. Laing, S. Schiff, and J.-Y. Wu, J. Neurosci. **44**, 9897 (2004).

[12] N. Wessel, J. Kurths, W. Ditto, and R. Bauernschmitt, Chaos **17**, 015101 (2007).

[13] B. J. Roth and A. M. Pertsov, Physica D **238**, 1019 (2009).

[14] S. Luther *et al.*, Nature **475**, 235 (2011).

[15] J. P. Keener and J. J. Tyson, SIAM Rev. **1**, 1 (1992).

[16] M. Vinson, S. Mironov, S. Mulvey, and A. Pertsov, Nature **386**, 477 (1997).

[17] C. Luengviriya and M. J. B. Hauser, Phys. Rev. E **77**, 056214 (2008).

[18] M. A. Bray and J. P. Wikswo, Phys. Rev. Lett. **90**, 238303 (2003).

[19] M. Gabbay, E. Ott, and P. N. Guzdar, Phys. Rev. E **58**, 2576 (1998).

[20] T. Bánsági Jr. and O. Steinbock, Phys. Rev. E **76**, 045202 (2007).

[21] R. M. Zaritski, S. F. Mironov, and A. M. Pertsov, Phys. Rev. Lett. **92**, 168302 (2004).

[22] Z. A. Jiménez, B. Marts, and O. Steinbock, Phys. Rev. Lett. **102**, 244101 (2009).

[23] Z. A. Jiménez and O. Steinbock, Europhys. Lett. **91**, 50002 (2010).

[24] S. Dutta and O. Steinbock, J. Phys. Chem. Lett. **2**, 945 (2011).

[25] T. Bánsági, Jr. and O. Steinbock, Phys. Rev. Lett. **97**, 198301 (2006).

[26] D. Margerit and D. Barkley, Chaos **12**, 636 (2002).

[27] A. M. Pertsov, M. Wellner, M. Vinson, and J. Jalife, Phys. Rev. Lett. **84**, 2738 (2000).

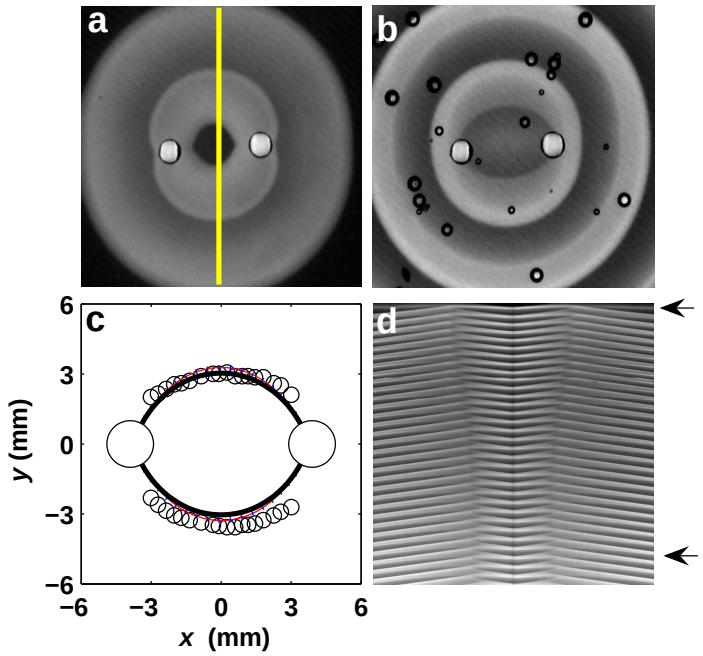

FIG. 1. (color online) Snapshots of a pinned scroll wave (a) 2 min and (b) 200 min after initiation. The spherical obstacles are 7.8 mm apart and 0.93 mm in radius. Field of view 20×20 mm^2. (c) Measured position of the stationary filament (small circles) and the corresponding simulations based on Eq. (2) (solid lines). The large circles represent the pinning spheres. (d) Space-time plot for the experiment in (a, b) extracted along the center line (yellow) in (a). Time evolves in downward direction spanning 227 min. Arrows denote the times at which the snapshots (a) and (b) were recorded.

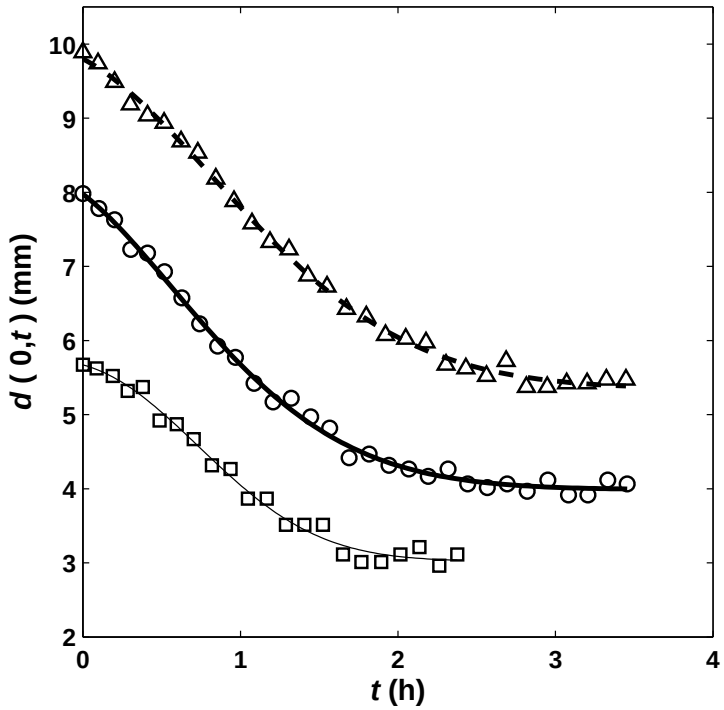

FIG. 2. Kinetics of the filament distance $d(x,t)$ as measured halfway (x=0) between the pinning sites. The smooth curves are fits with compressed exponentials. Distance between beads: 6.1 mm (squares), 6.4 mm (circles), and 7.0 mm (triangles). Bead radius: 1 mm in all three experiments.

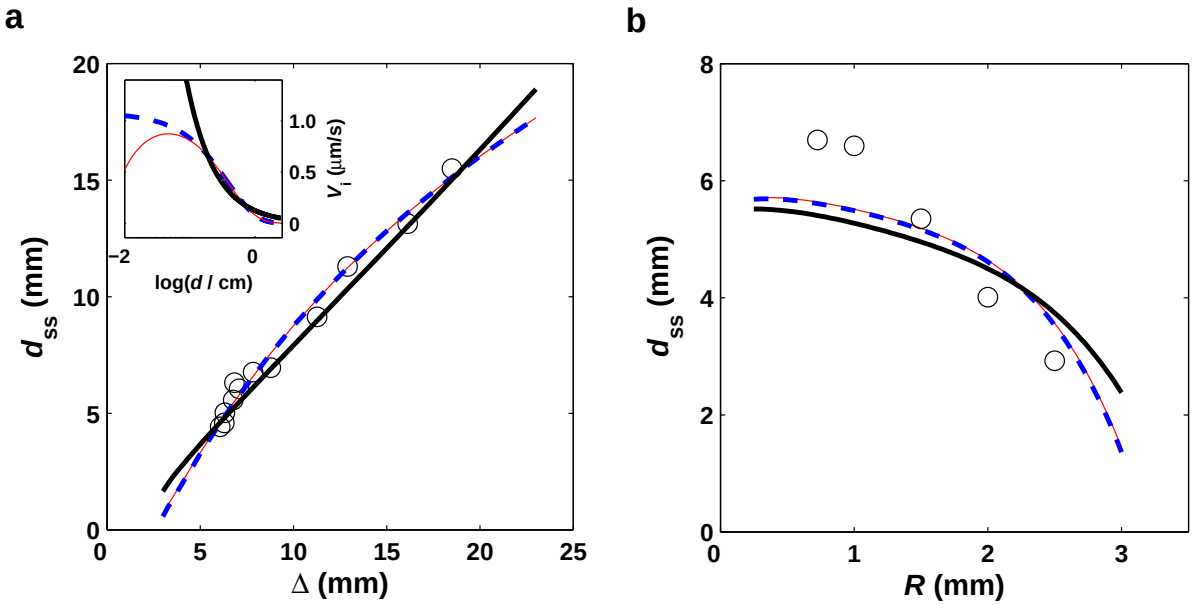

FIG. 3. (color online) Stationary filament distance d_{ss} as a function of (a) the distance between the spherical heterogeneities Δ and (b) their radius R. In (a) the heterogeneity radius R was kept constant at 1.0 mm; in (b) Δ was 6.8 ± 0.15 cm. The curves show numerical results based on Eq. (2) and distance-dependent interaction velocities described by the difference of two Yukawa potentials (thin solid line, red), an exponential function (dashed line, blue), and inverse proportionality (thick solid line, black). The three functions are shown in the inset.

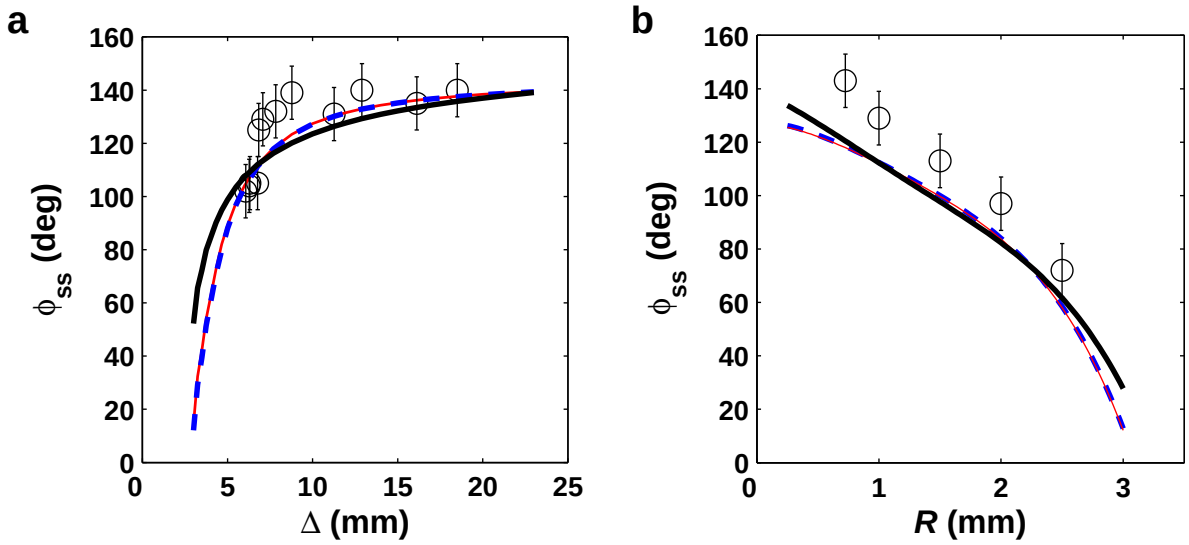

FIG. 4. (color online) Angle between the stationary filament branches close to the pinning surface as a function of (a) the distance between the spherical heterogeneities and (b) the heterogeneity radius. In (a) the heterogeneity radius R is kept constant at 1.0 mm; in (b) Δ is 6.8 $\pm$ 0.15 cm. The curves show numerical results based on Eq. (2) and three different interaction functions (see Fig. 3).